Title

A strain-driven thermotropic phase boundary in BaTiO3 at room temperature by cycling compression

Journal

AIP Advances, 11(11)

ISSN

2158-3226

Authors

Ren, Yifeng

Li, Jiayi

Zhao, Yunlei

et al.

Publication Date

2021-11-01

DOI

10.1063/5.0066660

A strain-driven thermotropic phase boundary in $BaTiO_3$ at room temperature by cycling compression

Cite as: AIP Advances 11, 115122 (2021); doi: 10.1063/5.0066660
Submitted: 15 August 2021 • Accepted: 3 November 2021 •
Published Online: 16 November 2021

Yifeng Ren,[1,2] Jiayi Li,[2,3] Yunlei Zhao,[1,2] Jim Ciston,[4] Karen Bustillo,[4] Ruopeng Zhang,[4,5] Hongliang Dong,[6] Zhiqiang Chen,[6,a)] Andrew M. Minor,[4,5] and Yu Deng[2,3 a)]

AFFILIATIONS

[1] School of Physics, Nanjing University, Nanjing 210093, China
[2] Solid State Microstructure National Key Lab and Collaborative Innovation Center of Advanced Microstructures, Nanjing University, Nanjing 210093, China
[3] Department of Materials Science and Engineering, College of Engineering and Applied Sciences, Nanjing University, Nanjing 210093, China
[4] National Center of Electron Microscopy, Molecular Foundry, Lawrence Berkeley National Laboratory, Berkeley, California 94720, USA
[5] Department of Materials Science and Engineering, University of California, Berkeley, California 94720, USA
[6] Center for High Pressure Science and Technology Advanced Research, Shanghai 201203, China

[a)] **Authors to whom correspondence should be addressed:** chenzq@hpstar.ac.cn and dengyu@nju.edu.cn

ABSTRACT

In $BaTiO_3$ single crystals, we observed a strain-driven phase transition from the tetragonal phase to the tetragonal-orthorhombic phase boundary which can be introduced by slow cycling compressions (a loading of up to 0.5 GPa, strain rate of 10^{-4} s^{-1}, and 100 cycles) at room temperature. Different from the well-known tetragonal to cubic phase transition under stress (~2 GPa), it only takes place locally around bent 90° domain walls. The inhomogeneous local stress and electrical fields as well as the mobile point defect pinning effect contribute to the phase re-entrance. Through comparison experiments by *in situ* synchrotron x-ray diffraction, Raman scattering, and (scanning) transmission electron microscopy, we explored the phase transition mechanism. Based on that, we developed a mechanical method to obtain well-stabilized high-density thermotropic phase boundary structures (with tetragonal, orthorhombic, and bridging monoclinic phases) in $BaTiO_3$ for potential applications.

For ferroelastic-ferroelectric materials (FMs), multiple phases coexisting at the phase boundary can significantly enhance their properties through a nonlinear effect caused by the complex microstructural interactions,[1–3] e.g., the surprisingly large piezoelectric effect in $BiFeO_3$ and $Pb(Mg_{0.33},Nb_{0.67})O_3$–$PbTiO_3$ at the morphotropic phase boundary.[4,5] Now they attract more research attention in actuator, memory, flexible/wearable electronic device, and piezoelectric nanogenerator fields.[6–10] Notably, from many FMs' phase diagrams, we can clearly see that almost none of the phase boundaries occur at room temperature and ordinary pressure;[11–16] therefore, in the past decades, much effort has been focused on how to introduce and then stabilize them for daily use, such as stress,[4] thermal and electrical methods, and composition doping.[4,16–18] Among them, the stress/strain method is particularly interesting: (1) Since stress is unscreenable in FMs, it can introduce extremely high-density domain walls and phase boundaries (for coexisting phases, each has its own domain structures[12,19]) which lead to excellent multiple phase interaction/coupling.[20] (2) Under non-hydrostatic pressure, the phase transition sequence heavily depends on the mechanical loading methods which provide more choices for tuning multiple phase structures.[21] Certainly, understanding the intrinsic mechanisms of domain and phase evolution

under stress loading is key.[8,22–26] Tracing the full domain growth and phase transition processes is needed to find the critical spatiotemporal features (which are commonly complicated hierarchical domain/phase structures[5,8]), which are largely shrouded in mystery.[25–29] Encouragingly, recent technology advances, such as the *in situ* (scanning) transmission electron microscope [(S)TEM] with atomic resolution imaging under nanoindentation,[30] fast direct detection device cameras, and synchrotron x-ray diffraction (XRD) with an accurate auto-loading *in situ* diamond anvil cell (DAC) system,[1] enable us to clearly record strain-driven hierarchical domain and phase evolutions. In this work, we designed a series of *in situ* experiments to clarify an "abnormal" strain-driven phase transition [toward a thermotropic phase boundary (TPB)] in $BaTiO_3$, where domain and multiple phase structures strongly interact. In addition, the microstructural mechanism has been discussed.

The bulk $BaTiO_3$ single crystal was purchased from Siccas, Shanghai. Synchrotron XRD was carried out at the Shanghai Synchrotron Radiation Facility (Shanghai, China), beam line 15U1, at room temperature (300 K). The single crystal $BaTiO_3$ sample was sealed in a DAC. An x-ray beam with 20 keV energy, 0.6199 Å wavelength, and a beam size of 3–5 μm was used. Notably, the single crystal sample in the DAC inevitably undergoes cracking and grain rotation during non-hydrostatic compression cycling, leading to polycrystalline-like XRD patterns. About the XRD results, the data in Fig. 1 were treated by masking and refining with DIOPAS software. Raman scattering was performed using a Renishaw inVia system (a 532 nm excitation laser source), with an auto-loading *in situ* DAC. Before being put into the DAC, single crystal $BaTiO_3$ was cut by laser. (S)TEM investigations were carried out by using a Cs-corrected (S)TEM, Thermo Fisher, with a K2-IS DDD camera, Gatan, and an *in situ* nanoindentation holder, PI-95, Hysitron. For *in situ* TEM study, a $BaTiO_3$ sub-micrometer pillar was prepared by focused ion beam.

Synchrotron XRD results (Fig. 1) show a subtle phase transition in single crystal $BaTiO_3$ under slow non-hydrostatic cycling compression (a maximum engineering stress of 0.5 GPa and average loading/unloading rate of 10^{-4} s^{-1}). The diffraction peaks changed at {111} and {200}, after more compression cycles (the XRD curves were measured after unloading). As shown in the right inset of Fig. 1, the width of the {111} peak becomes broader, and the intensities of the two shoulder peaks of {200} get closer, exhibiting a typical symbol for tetragonal (T, *P4mm*, a = 3.9925 Å, and b = 4.0365 Å) to orthorhombic (O, *Amm*2, a = 3.9874 Å, b = 5.6751 Å, and c = 5.6901 Å) phase transition in $BaTiO_3$.[31] As known, during the T-O phase transition, the XRD multiple peaks at 11.78°–11.82°, which look similar to a single "broad peak," should display an obvious broadening owing to the further splitting of the multiple peaks.[16,31] Here, we have recorded the broadening of the multiple peaks (the shoulder), as shown in the right inset of Fig. 1, evidently approving the T-O phase transition in $BaTiO_3$. Considering the classical phase transition sequence of $BaTiO_3$ by hydrostatic pressure, i.e., from T to cubic (C),[11,32] the phase transition here is "abnormal." As known, recent theoretical and experimental reports predicted that the T-O phase transition inclines, leading to a wide TPB composed of T, O, and a bridging monoclinic (M) phase,[16,19,31] where the local inhomogeneous fields and domain structures are responsible for the stable multiple phase structures.[19] As expected, we find that the cycling-induced phase structure is well stabilized after unloading, even for weeks. Such domain/phase structures should be useful if they are stable under electrical excitation and over a broad temperature range.

To further verify the abnormal phase transition, we performed Raman scattering (more sensitive to detect multiple phase evolution) on the $BaTiO_3$ sample inside the DAC (also measured after unloading). Figure 2 (iii)–(v) (see the right inset's enlarged view) demonstrate the T to O phase transition. As cycling goes on, we find that the A1(TO1) (~240 to 270 cm^{-1}) peak down-shifts and its intensity increases, accompanied with an obvious broadening. In addition, the TO3 (~300 to 320 cm^{-1}) peak up-shifts, and its intensity decreases. Clearly, the phase structure does not transit toward the cubic one, which leads to a paraelectric type of Raman spectrum, as shown in Fig. 2(i), with only two weak peaks of A1(TO1) and TO3. Moreover, the E(TO4) (~485 cm^{-1}) peak emerges, implying that there is multiple phase coexistence. In addition, we find no rhombohedral (R) phase here. The typical R phase Raman peaks of E(TO1) and TO2-LO2 [~160 to 200 cm^{-1}, the intensive ones in Fig. 2 (vi) and (vii)] are not detectable at all.[32] Therefore,

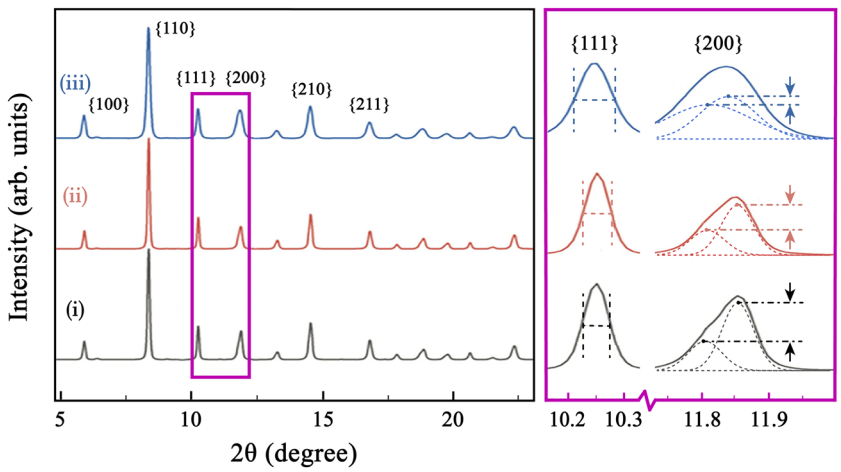

FIG. 1. Synchrotron XRD results of a $BaTiO_3$ single crystal inside an auto-loading DAC measured (i) before and (ii) after 30 cycles and (iii) 100 cycles of compressions, with corresponding direct diffraction patterns given beside. The right inset shows an enlarged view of {111} and {200} diffraction peaks, for knowing their variations in detail.

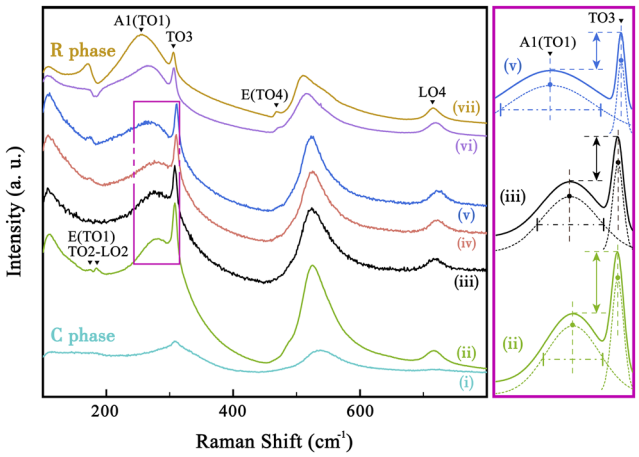

FIG. 2. Raman spectra of the $BaTiO_3$ single crystal inside a DAC for comparison study, before compression cycling at (i) 450 K (C phase), (ii) 300 K (room temperature), (vi) and (vii) 200 and 150 K (R phase), and at room temperature after (iii)–(v) 30, 60, 100 cycles, respectively. The right inset shows an enlarged view of A1(TO1) and TO3 in (ii), (iii), and (v), with multiple peak fitting (the peak frequency, width, and relative intensity are highlighted with dotted lines).

we suggest that a TPB at the T-O phase boundary has been introduced in $BaTiO_3$.[16,31–35] The phase transition should be regarded as a phase re-entrance, which has been reported in such a nanostructure and highly strained system of FMs.[21,32,35–37]

As known for multi-phase-coexisting microstructures at $BaTiO_3$'s T-O phase boundary, there have been long-time controversies, e.g., the adaptive phase theory, which denies the bridging M phase and attributes the macroscale, measured the "new phase" to the average effect,[5,38] and even recent theoretical and experimental research, which confirmed the bridging phase, also declared that the phase is not a classically defined one but with a flexible lattice structure.[16,19,31] To understand the phase transition at the T-O phase boundary, we have traced the microstructural evolutions. Figure 3 exhibits an *in situ* TEM study on a free-standing single crystal $BaTiO_3$ sub-micrometer pillar, which acts as a model sample to show what happened at atomic resolution during the non-hydrostatic cycling.

Under large compression, single crystal $BaTiO_3$ inevitably displays local shearing to release stress, e.g., via inhomogeneous local strain distribution and ultrasmall domain evolution.[4,8] As a result, the abnormal phase transition has been triggered locally, accompanied by a domain wall pinning effect,[8,39] explained step by step as follows [see Fig. 3(b) (i)–(v)]:

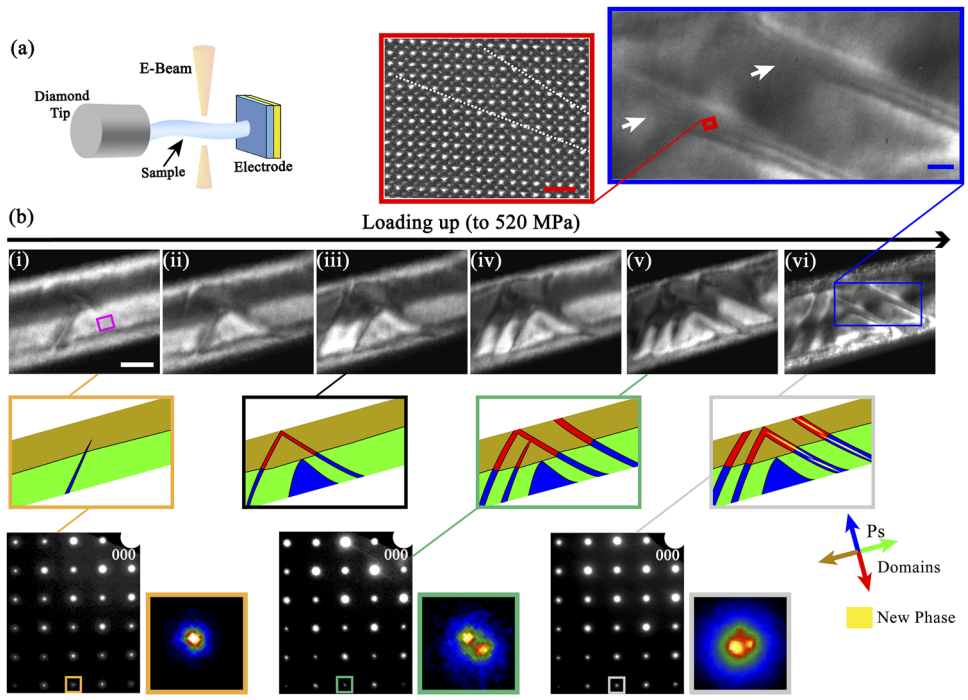

FIG. 3. (a) Setup of the *in situ* (S)TEM. (b) (i)–(vi) *In situ* observation of a single crystal $BaTiO_3$ sub-micrometer pillar under its 30th cycle compression, loaded up to 520 MPa (axial engineering stress). The dark-field TEM operation vector g = 404. For (i), (iii), (v), and (vi), the corresponding domain and phase structures are represented by simplified models below, and the lowest insets illustrate the SAED results of the pillar (pink-framed region), with an enlarged view showing the diffraction spot splitting. Here, only 1/4 SAED patterns are shown. For (vi), two upper right insets show the zoomed-in morphological view (by the white arrows) and a further zoomed-in HRSTEM view around a 90° domain wall, evidently exhibiting a multiple phase structure (white dotted lines highlight the phase boundaries). The white, blue, and red scale bars are 100, 20, and 1 nm, respectively.

(1) Under loading, typical herringbone domain structures composed of 90° and 180° domains are observed, and the bent domain walls (as the simplified models show) are related to local shearing, which also causes bending contours (as dark-field TEM images show) in the pillar.

(2) Notably, we find no domain side growth (i.e., two domain walls of one domain move laterally in opposite directions) or merging (i.e., domain walls disappear) during the domain evolution, implying that they are strongly impeded after domain nucleation and forward growth [as shown in (i)–(vi)].[8] It should be connected with mobile point defects, i.e., the pinning centers, which accumulate at the bent 90° domain walls for charge neutrality and subsequently pin the domain walls from lateral motion or merging.[11,40–42] The intrinsic electrostatic potential drop across the 90° domain wall (instead of the 180° one) creates electric fields and cause charged defects aggregating on different sides of the domain wall.[43,44] In addition, the strain–charge interaction can greatly enhance this defect accumulation effect, under stress loading,[45] and long-time cycling is responsible for accumulation of mobile point defects.[8] Moreover, without domain merging, it inevitably causes domain miniaturization,[5,46,47] which in turn promotes large local shearing in $BaTiO_3$ ($w_{ac} \approx G^{-1/2}$, w_{ac} is polytwin's periodicity and G is the local shear strain[48,49]).

(3) As loading further increased, some ultrathin microstructures appeared at 90° domain walls [see (vi) in Fig. 3(b)]. Topologically, the morphology (shown by white arrows) cannot be classified as any domain structure of T phase $BaTiO_3$.[50] In addition, the selected area electron diffraction (SEAD) shows that there is a new induced phase, with a splitting diffraction spot beside the 90° domain. In good agreement, the atomic resolution observation (the blue-framed inset) reveals that the phase boundaries (denoted by white dotted lines) obviously belong neither to the T nor to the O phase domain wall geometry.[16] It indicates there is a bridging M phase at the T-O phase boundary (a TPB). In addition, they is no composition changing (see the supplementary material).

Figure 4 schematically shows the strain-driven TPB at a 90° domain wall in $BaTiO_3$. The abnormal phase transition (a phase reentrance) takes place locally around bent domain walls (as well as stressed surfaces),[32,35] where local stress/electrical fields play critical roles.[8,48] Here, the compression loading (engineering stress of up to 520 MPa) is not enough to trigger any global phase transition (~2.3 GPa for $BaTiO_3$[32]), and the long-time (~10^2 cycles, with loading rate ~10^{-4} s^{-1}) non-hydrostatic compression cycling is also essential: it not only stabilizes the stress-introduced domain walls and phase boundaries via mobile point defect pinning effect (see Fig. 4, where mobile point defects accumulate at the 90° domain walls)[19,41,42] but also impedes domain side growth and merging, therefore causing domain miniaturization (it in turn promotes local shearing) and providing more domain walls for TPB nucleation.[8]

Based on the above-mentioned discussions, we believe we have found a way to mechanically induce a TPB into $BaTiO_3$ at room temperature. Compared with electrical and thermal methods, the stress method is good at introducing extremely high-density domain walls and phase boundaries (since the stress is unscreenable in FMs), greatly promoting multiple phase coupling.[51] It is worth pointing out that "proper" compression cycling parameters are critical to avoid possible material failure: for fracture-free engineering, the loading must be slow enough (e.g., ~10^{-4} s^{-1}), and loading maximum should not be too high (e.g., ≤600 MPa[52]). Here, small size greatly favors mechanical engineering since it contributes to both FMs' flexibility and domain miniaturization (high-density domain walls enable high-density TPB structures because they are TPB nucleation sites[8,20]). In addition, selecting a proper temperature is also effective in tuning the strain-driven phase transition pathways and subsequently the TPB structures.[21,53]

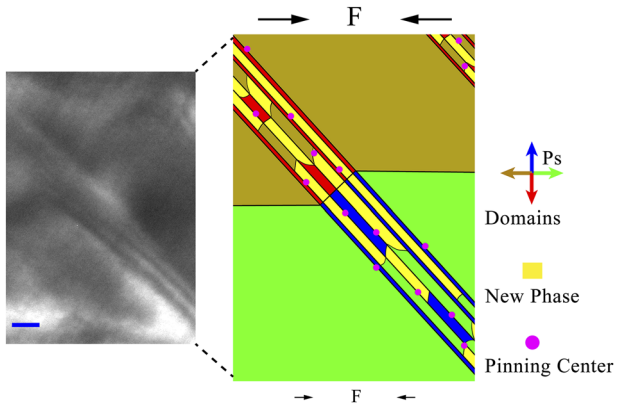

FIG. 4. Schematic diagram for the strain-driven TPB around a 90° domain wall. Here, the geometry of the TPB and T phase domain is a result of phase field simulation (for the method, see Ref. 8). The "New Phase" actually includes both O and M phases, which can be introduced simultaneously during the phase transition.[16] The phase and domain structures (with local shearing) correspond to Fig. 3(b)(vi). The blue scale bar is 20 nm.

SUPPLEMENTARY MATERIAL

See the supplementary material for the sensitive Electron Energy Loss Spectroscopy (EELS) at domain and domain walls, before and after domain/phase transition, showing no edge variation, and the results illustrate that they do not change in composition.

ACKNOWLEDGMENTS

Y.D. acknowledges the Natural Science Foundation of Jiangsu Province, China (Grant No. BK20201246); Z.C. acknowledges the National Natural Science Foundation of China (Grant No. U1530402); and H.D. acknowledges the Shanghai Synchrotron Radiation Facility (SSRF) BL 15U1.

AUTHOR DECLARATIONS

Conflict of Interest

The authors have no conflicts to disclose.

Author Contributions

Y.R. and J.L. contributed equally to this work.

DATA AVAILABILITY

The data that support the findings of this study are available from the corresponding authors upon reasonable request.

REFERENCES

[1]M. Ahart, M. Somayazulu, R. E. Cohen, P. Ganesh, P. Dera, H.-k. Mao, R. J. Hemley, Y. Ren, P. Liermann, and Z. Wu, Nature **451**(7178), 545 (2008).
[2]R. E. Newnham, Mater. Res. Soc. Bull. **22**, 20 (1997).
[3]J. Fu, H. Qi, A. Xie, A. Tian, and R. Zuo, Acta Mater. **215**, 117100 (2021).
[4]R. J. Zeches, M. D. Rossell, J. X. Zhang, A. J. Hatt, Q. He, C.-H. Yang, A. Kumar, C. H. Wang, A. Melville, C. Adamo, G. Sheng, Y.-H. Chu, J. F. Ihlefeld, R. Erni, C. Ederer, V. Gopalan, L. Q. Chen, D. G. Schlom, N. A. Spaldin, L. W. Martin, and R. Ramesh, Science **326**(5955), 977 (2009).
[5]Y. M. Jin, Y. U. Wang, A. G. Khachaturyan, J. F. Li, and D. Viehland, J. Appl. Phys. **94**(5), 3629 (2003).
[6]L. Zhang, W. Liu, W. Chen, X. Ren, J. Sun, E. A. Gurdal, S. O. Ural, and K. Uchino, Appl. Phys. Lett. **101**(24), 242903 (2012).
[7]H. Lu, C.-W. Bark, D. Esque de los Ojos, J. Alcala, C. B. Eom, G. Catalan, and A. Gruverman, Science **336**(6077), 59 (2012).
[8]Y. Deng, C. Gammer, J. Ciston, P. Ercius, C. Ophus, K. Bustillo, C. Song, R. Zhang, D. Wu, Y. Du, Z. Chen, H. Dong, A. G. Khachaturyan, and A. M. Minor, Acta Mater. **181**, 501 (2019).
[9]Z.-H. Lin, Y. Yang, J. M. Wu, Y. Liu, F. Zhang, and Z. L. Wang, J. Phys. Chem. Lett. **3**(23), 3599 (2012).
[10]S. H. Baek, J. Park, D. M. Kim, V. A. Aksyuk, R. R. Das, S. D. Bu, D. A. Felker, J. Lettieri, V. Vaithyanathan, S. S. N. Bharadwaja, N. Bassiri-Gharb, Y. B. Chen, H. P. Sun, C. M. Folkman, H. W. Jang, D. J. Kreft, S. K. Streiffer, R. Ramesh, X. Q. Pan, S. Trolier-McKinstry, D. G. Schlom, M. S. Rzchowski, R. H. Blick, and C. B. Eom, Science **334**(6058), 958 (2011).
[11]J. íñiguez and D. Vanderbilt, Phys. Rev. Lett. **89**(11), 115503 (2002).
[12]N. Jaykhedkar, N. Tripathy, V. Shah, B. Pujari, and S. Premkumar, Mater. Chem. Phys. **254**, 123545 (2020).
[13]T. Asada and Y. Koyama, Phys. Rev. B **75**(21), 214111 (2007).
[14]J. Gao, D. Xue, Y. Wang, D. Wang, L. Zhang, H. Wu, S. Guo, H. Bao, C. Zhou, W. Liu, S. Hou, G. Xiao, and X. Ren, Appl. Phys. Lett. **99**(9), 092901 (2011).
[15]C. L. Bull, C. J. Ridley, K. S. Knight, N. P. Funnell, and A. S. Gibbs, Mater. Adv. **2**(18), 6094 (2021).
[16]T. T. A. Lummen, Y. Gu, J. Wang, S. Lei, F. Xue, A. Kumar, A. T. Barnes, E. Barnes, S. Denev, A. Belianinov, M. Holt, A. N. Morozovska, S. V. Kalinin, L.-Q. Chen, and V. Gopalan, Nat. Commun. **5**, 3172 (2014).
[17]J. X. Zhang, B. Xiang, Q. He, J. Seidel, R. J. Zeches, P. Yu, S. Y. Yang, C. H. Wang, Y.-H. Chu, L. W. Martin, A. M. Minor, and R. Ramesh, Nat. Nanotechnol. **6**(2), 98 (2011).
[18]R. E. Cohen, Nature **441**(7096), 941 (2006).
[19]Y. J. Gu, F. Xue, S. M. Lei, T. T. A. Lummen, J. J. Wang, V. Gopalan, and L. Q. Chen, Phys. Rev. B **90**(2), 024104 (2014).
[20]G. Catalan, J. Seidel, R. Ramesh, and J. F. Scott, Rev. Mod. Phys. **84**(1), 119 (2012).
[21]M. Guennou, P. Bouvier, G. S. Chen, B. Dkhil, R. Haumont, G. Garbarino, and J. Kreisel, Phys. Rev. B **84**(17), 174107 (2011).
[22]J. Chen, J. E. Daniels, J. Jian, Z. Cheng, J. Cheng, J. Wang, Q. Gu, and S. Zhang, Acta Mater. **197**, 1 (2020).
[23]S. Zhu, M. Yang, X. Gu, P. Zhou, and C. Zhong, Comput. Mater. Sci. **181**, 109713 (2020).
[24]X. Zhou, H. Marion, L. M. Riemer, E. Bruder, B. Liu, L. Zhou, P. B. Groszewicz, F. Zhuo, B.-X. Xu, K. Durst, X. Tan, D. Damjanovic, J. Koruza, and J. Rödel, Science **372**, 961 (2021).
[25]J. M. Gregg, Science **336**(6077), 41 (2012).
[26]V. Stepkova, P. Marton, and J. Hlinka, J. Phys.: Condens. Matter **24**(21), 212201 (2012).
[27]S. Yang, H. Bao, C. Zhou, Y. Wang, X. Ren, Y. Matsushita, Y. Katsuya, M. Tanaka, K. Kobayashi, X. Song, and J. Gao, Phys. Rev. Lett. **104**(19), 197201 (2010).
[28]R. Liu, J. G. Ulbrandt, H.-C. Hsing, A. Gura, B. Bein, A. Sun, C. Pan, G. Bertino, A. Lai, K. Cheng, E. Doyle, K. Evans-Lutterodt, R. L. Headrick, and M. Dawber, Nat. Commun. **11**(1), 2630 (2020).
[29]N. Bassiri-Gharb, Science **369**(6501), 252 (2020).
[30]Y. He, L. Zhong, F. Fan, C. Wang, T. Zhu, and S. X. Mao, Nat. Nanotechnol. **11**(10), 866 (2016).
[31]L. Kong, G. Liu, W. Yang, and W. Cao, Appl. Phys. Lett. **107**(4), 042901 (2015).
[32]W. Han, J. Zhu, S. Zhang, H. Zhang, X. Wang, Q. Wang, C. Gao, and C. Jin, J. Appl. Phys. **113**(19), 193513 (2013).
[33]U. D. Venkateswaran, V. M. Naik, and R. Naik, Phys. Rev. B **58**(21), 14256 (1998).
[34]J. P. Itié, B. Couzinet, A. Polian, A. M. Flank, and P. Lagarde, Europhys. Lett. **74**(4), 706 (2006).
[35]X. Wang, X. Deng, H. Wen, and L. Li, Appl. Phys. Lett. **89**(16), 162902 (2006).
[36]J. Zhu, C. Jin, W. Cao, and X. Wang, Appl. Phys. Lett. **92**(24), 242901 (2008).
[37]S. Lin, L. Tianquan, C. Jin, and X. Wang, Phys. Rev. B **74**(13), 134115 (2006).
[38]A. G. Khachaturyan and G. Shatalov, Sov. Phys. JETP **29**(3), 557 (1969).
[39]X. Ren, Nat. Mater. **3**(2), 91 (2004).
[40]C. Eisenschmidt, H. T. Langhammer, R. Steinhausen, and G. Schmidt, Ferroelectrics **432**(1), 103 (2012).
[41]Y. Xiao, V. B. Shenoy, and K. Bhattacharya, Phys. Rev. Lett. **95**(24), 247603 (2005).
[42]Y. Zhang, J. Li, and D. Fang, Phys. Rev. B **82**(6), 064103 (2010).
[43]L. Hong, A. K. Soh, Q. G. Du, and J. Y. Li, Phys. Rev. B **77**(9), 094104 (2008).
[44]X. Wang, T. Xu, F. Xuan, C. Chen, T. Shimada, and T. Kitamura, J. Appl. Phys. **126**(17), 174107 (2019).
[45]H. Elangovan, M. Barzilay, J. Huang, S. Liu, S. Cohen, and Y. Ivry, ACS Nano **15**, 13380 (2021).
[46]Y. Ivry, J. F. Scott, E. K. H. Salje, and C. Durkan, Phys. Rev. B **86**(20), 205428 (2012).
[47]Y. Ivry, D. Chu, and C. Durkan, Appl. Phys. Lett. **94**(16), 162903 (2009).
[48]J. Paul, T. Nishimatsu, Y. Kawazoe, and U. V. Waghmare, Phys. Rev. B **80**(2), 024107 (2009).
[49]Y. Ivry, D. P. Chu, and C. Durkan, Nanotechnology **21**(6), 065702 (2010).
[50]N. T. Tsou, P. R. Potnis, and J. E. Huber, Phys. Rev. B **83**(18), 184120 (2011).
[51]M. Daraktchiev, G. Catalan, and J. F. Scott, Phys. Rev. B **81**(22), 224118 (2010).
[52]Y. Gaillard, A. H. Macías, J. Muñoz-Saldaña, M. Anglada, and G. Trápaga, J. Phys. D: Appl. Phys. **42**(8), 085502 (2009).
[53]Y. L. Li and L. Q. Chen, Appl. Phys. Lett. **88**(7), 072905 (2006).